Stratiform precipitation, vertical heating profiles, and the Madden-Julian Oscillation

Jialin Lin[1,2*] Brian Mapes[1], Minghua Zhang[2] and Matthew Newman[1]
[1] *NOAA-CIRES Climate Diagnostics Center, Boulder, Colorado*
[2] *State University of New York, Stony Brook, New York*

(Manuscript received 20 November 2002, in final form 12 June 2003)

ABSTRACT

The observed profile of heating through the troposphere in the Madden-Julian Oscillation (MJO) is found to be very top-heavy: more so than seasonal-mean heating, and systematically more so than all of the seven models for which intraseasonal heating anomaly profiles have been published. Consistently, the Tropical Rainfall Measurement Mission (TRMM) Precipitation Radar shows that stratiform precipitation (known to heat the upper troposphere and cool the lower troposphere) contributes more to intraseasonal rainfall variations than it does to seasonal-mean rainfall. Stratiform rainfall anomalies lag convective rainfall anomalies by a few days. Reasons for this lag apparently include increased wind shear and middle-upper tropospheric humidity, which also lag convective (and total) rainfall by a few days.

A distinct rearward tilt is seen in anomalous heating time-height sections, in both the strong December 1992 MJO event observed by the Tropical Ocean Global Atmosphere Coupled Ocean-Atmosphere Response Experiment (TOGA COARE) and a composite MJO constructed from multi-year data sets. Interpretation is aided by a formal partitioning of the COARE heating section into convective, stratiform, and radiative components. The tilted structure after the maximum surface rainfall appears to be contributed largely by latent and radiative heating in enhanced stratiform anvils. However, the tilt of anomalous heating ahead of maximum rainfall is seen within the convective component, suggesting a change from shallower to deeper convective heating as the wet phase of the MJO approached the longitude of the observations.

1. Introduction

Discovered by Madden and Julian (1971, 1972), the Madden-Julian Oscillation (MJO) is the dominant intraseasonal mode of variability in tropical convection and circulation (e.g. Weickmann et al. 1985, Lau and Chan 1985, Salby and Hendon 1994, Wheeler and Kiladis 1999). It affects a wide range of tropical weather such as the onset and breaks of the Indian and Australian summer monsoons (e.g. Yasunari 1979, Hendon and Liebmann 1990), and the formation of tropical cyclones (e.g. Nakazawa 1986, Liebmann et al. 1994). It also drives teleconnections to the extratropics (e.g., Lau and Phillips 1986, Winkler et al. 2001) and impacts some important extratropical weather (e.g. Higgins and Mo 1997, Higgins et al. 2000). On a longer timescale, the MJO is observed to trigger or terminate some El Nino events (e.g. Kessler et al. 1995, Takayabu et al. 1999, Bergman et al. 2001). Therefore, the MJO is important for both extended-range weather forecasting and long-term climate prediction.

The MJO is concentrated in the eastern hemisphere. Figure 1a shows the standard deviation of 30-70 day bandpass filtered precipitation (from CMAP, see section 2 and 3 for details of data and filtering). This intraseasonal rainfall variability has two heating centers, in the Indian ocean and the western Pacific. Eastward propagation is prominent, as seen in lagged correlations between a filtered time series of precipitation at 0N155E and precipitation elsewhere along the equator (Fig. 1b). The propagating part of intraseasonal variability (hereafter called the MJO) moves eastward from the Indian Ocean to the western Pacific, with a phase speed of about 5 m/s (4 degrees/day).

Eastward-propagating intraseasonal signals do occur in some general circulation models (GCMs), but are generally too weak and propagate too fast compared with observations (e.g. Hayashi and Sumi 1986, Hayashi and Golder 1986, 1988, Lau et al. 1988, Slingo et al. 1996). In light of the MJO's importance, reviewed above, this shortcoming is detrimental to both numerical weather prediction and climate prediction. The overarching goal of this work is

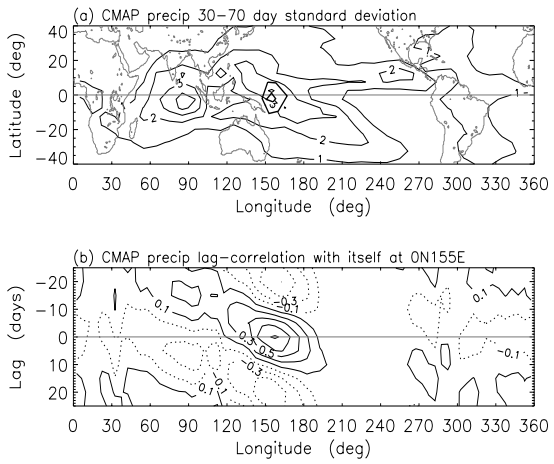

Figure 1: (a) Standard deviation of the 30-70 day bandpass filtered anomaly of the CMAP precipitation from 1979-2002. The unit is mm/day. The thick solid polygons are the sounding arrays during TOGA COARE. The inner one is the Intensive Flux Array (IFA). The outer one is the Outer Sounding Array (OSA). (b) The lag-correlation between the 30-70 day CMAP precipitation anomaly and itself at 0N155E.

to contribute to improved GCM simulations of tropical variability. A first step toward that goal is to better document the observed phenomenon, in order to better define the form and (hopefully) nature of model errors.

Diabatic heating (mainly latent and radiative) is central to the structure and propagation of the MJO (Krishnamurti et al. 1985, Murakami and Nakazawa 1985, Yanai et al. 2000). The heating is strongly associated with a propagating large-scale circulation anomaly (hereafter called a 'wave'), which in turn feeds back onto the heating (Hendon and Salby 1994, Zhang 1996). This suggests the utility of a "wave-heating feedback" theoretical framework, of which many versions have been explored, with various degrees and types of approximations.

The vertical profile of heating has a large effect on intraseasonal oscillations in such wave-heating theoretical models (discussed further in section 7). In light of this sensitivity to heating profiles, it seems useful to document the observed MJO heating profile, and compare it to the same quantity in models. Might the models' difficulty in simulating the MJO be related to systematic error in model heating profiles?

Heating profiles over the tropical oceans have been measured as heat budget residuals, using sounding-array data in field experiments such as the Marshall Islands (Yanai et al. 1973), GATE (e.g. Thompson et al. 1979), AMEX (e.g. Frank and McBride 1989), and TOGA COARE (Lin and Johnson 1996, Frank et al. 1996, Yanai et al. 2000, and Zhang and Lin 1999). The profile of total heating in convecting regions is top-heavy, or concentrated high in the upper troposphere. This top-heaviness is contributed to by vertical dipole heating profiles observed in areas of stratiform precipitation, with heating in the upper troposphere and cooling in the lower troposphere (Houze 1982, 1989, 1997; Johnson 1984; Mapes and Houze 1995). Stratiform precipitation also lags convective precipitation in time, which might introduce important time-dependence to total heating profiles.

The anomalous vertical heating profile as it varies across the MJO has not been isolated in the published literature. As we shall see, it differs significantly from time-mean profiles. Likewise, the contribution of stratiform precipitation to mean precipitation has been studied (e.g. Schumacher and Houze 2003), but the contribution of anomalous stratiform precipitation to the anomalous precipitation in the MJO has not been reported. This study aims to remedy this lack, as a starting point to identify model errors.

The purpose of this study is to examine the observed anomalous heating profiles and stratiform precipitation in the MJO, consider the consistency of these completely independent measurements, and compare the observed heating profiles with those in some models. Major issues we address are:
(1) What is the vertical heating profile in the MJO? How does it compared with the climatological mean profile? How large does stratiform precipitation contribute to the vertical heating profile?
(2) How does the MJO vertical heating profile vary with time? Is it simply a reversing sign of a fixed profile, or is there phase tilt? If so, what factors contribute to this tilt?
(3) How well do current GCMs represent the vertical heating profile in the MJO?

The datasets used in this study are described in section 2. The methods are described in section 3. The anomalous vertical heating profiles in the convectively active phase are examined in section 4. The vertical phase tilt of heating anomaly is studied in section 5. Comparisons between the observed heating profiles and the GCM profiles are conducted in section 6. Summary and discussion are given in section 7.

2. Data

The datasets used include TOGA COARE data and long-term data.

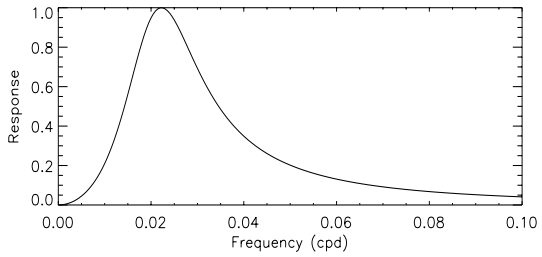

Figure 2: The response function of the Murakami filter used in this study.

The TOGA COARE datasets include:
(1) 120 day (November 1, 1992 to February 28, 1993) of the 6-hourly sounding array budgets for the Intensive Flux Array (IFA, Fig. 1) calculated by Ciesielski et al. (2002). The variables we used include diabatic heating Q_1, moisture sink Q_2, wind, horizontal divergence, and relative humidity.
(2) 120 day (November 1, 1992 to February 28, 1993) of the daily diabatic heating Q_1 profiles for the Outer Sounding Array (OSA, Fig. 1) calculated by Zhang and Lin (1999) using the method of Zhang and Lin (1997).
(3) 120 day (November 1, 1992 to February 28, 1993) of the hourly radiative heating Q_R profiles for the IFA Calculated by Qian and Cess (2003).

The long term datasets include:
(1) 24 years (1979-2002) of the pentad "chi-corrected" diabatic heating Q_1 profiles calculated by Sardeshmukh et al. (1999) and Winkler et al. (2001). The horizontal resolution is 2.5 degree longitude by 2.5 degree latitude. We average the data between 5N and 5S in longitudes 145-155E. These diabatic heating profiles are determined from an improved iterative solution of the "chi problem" (Sardeshmukh 1993), applied to four times daily NCEP reanalysis wind fields to minimize the nonlinear vorticity budget imbalance at 28 atmospheric levels. The modified divergence is further constrained to satisfy the large-scale mass budget. Diabatic heating rates are finally determined as a residual in the heat budget, using the modified wind circulation to compute advective terms. See Sardeshmukh (1993) for more details of the technique.
(2) 24 years (1979-2002) of NCEP reanalysis upper air wind data. The horizontal resolution is 2.5 degree longitude by 2.5 degree latitude. We average the data along the equator (between 5N and 5S) with a zonal resolution of 10 degree longitude.
(3) 24 years (1979-2002) of the pentad CPC Merged Analysis of Precipitation (CMAP) calculated by Xie and Arkin (1997). The horizontal resolution is 2.5 degree longitude by 2.5 degree latitude. We average the data along the equator (between 5N and 5S) with a zonal resolution of 5 degree longitude.
(4) 5 years (1998-2002) of the half-hourly TRMM precipitation radar (PR) gridded convective/stratiform precipitation (product number 3G68) calculated by Kummerow et al. (2000) and Stocker et al. (2001). The horizontal resolution is 0.5 degree longitude by 0.5 degree latitude. We average the data along the equator (between 5N and 5S) to pentad data with a zonal resolution of 10 degree longitude.
(5) Five years (1998-2002) of twice-daily upper air sounding data at the Atmosphere Radiation Measurement (ARM) Manus site located at 2S147E. We only use the relative humidity in this study. The data are averaged to pentad means. There are only a few missing pentads and they are filled using linear interpolation in time.

3. Method

The MJO is a broad-band phenomenon, with an averaged period of 45 days but a fairly wide spread from 20 to 80 days (see review by Madden and Julian 1994). Its deep convection signal is dominated by wavenumber 1-6, while its circulation signal is dominated by wavenumber 1 (e.g. Salby and Hendon 1994, Wheeler and Kiladis 1999). These characteristics are used to isolate the MJO signal as a master time series from space-time data.

Many different indices have been used in previous observational and modeling studies. Some are based on circulation signals (e.g. Madden and Julian 1972, Knutson and Weickmann 1987, Lau et al. 1988), others on deep convection signals (e.g. Lau and Chan 1985, Hendon and Salby 1994, among many others), while some use a combination of circulation and deep convection signals (e.g. Hsu 1996). Even in the case of a single variable (often OLR), various methods have been used to construct an MJO index, such as: (1) band-pass filtering and selection of a (usually large) grid box as the reference point (e.g. Lau and Chan 1985, Kiladis and Weickmann 1992, Zhang 1996, Woolnough et al. 2000); (2) band-pass filtering and selection of the leading Empirical Orthogonal Functions (EOFs) of the anomaly (e.g. Weickmann 1983, Lau and Chan 1985); (3) band-pass filtering and selection of strong, eastward propagating events (e.g. Rui and Wang 1990); and (4) space-time filtering to isolate only large-scale eastward propagating signals (e.g. Hendon and Salby 1994). The different methods often give qualita-

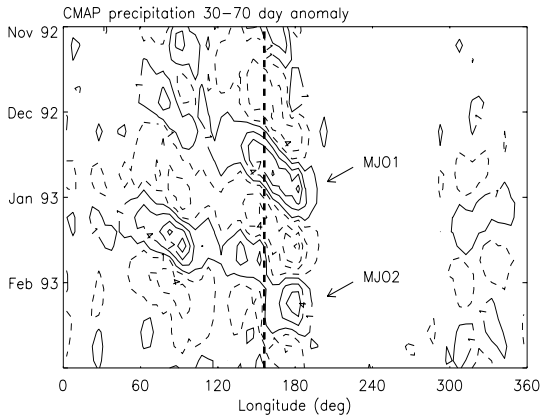

Figure 3: The 30-70 day bandpass filtered anomaly of the CMAP precipitation during TOGA COARE (November 1, 1992 to February 28, 1993). The unit is mm/day. The thick dashed line indicates the location of the TOGA COARE sounding arrays.

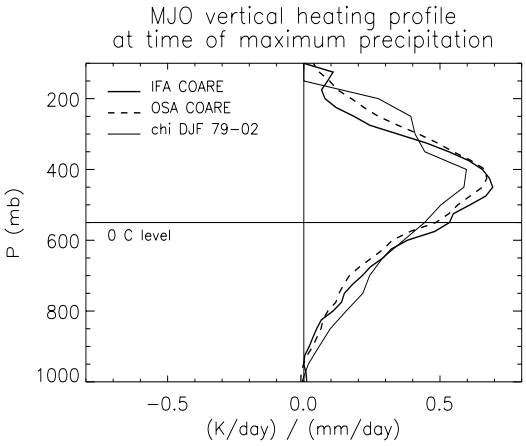

Figure 4: The MJO anomalous vertical heating profile at the time of maximum precipitation for TOGA COARE IFA (thick solid line), TOGA COARE OSA (thick dashed line), and DJF composite of 24 years (1979-2002) chi-corrected heating data at 0N155E (thin solid line).

tively similar results in terms of propagation characteristics and phase difference among different variables (e.g. Lau and Chan (1985) compared methods (1) and (2)). This consistency is apparently because strong intraseasonally filtered OLR fluctuations along the equator are dominated, both in number and strength, by coherent eastward propagating events (Wang and Rui 1990a). Linear composite methods used in most of the previous studies (e.g. phase sum, correlation, regression) are apparently dominated by these strong eastward propagating events.

This study uses the above method (1). All datasets are filtered using a 30-70 day Murakami (1976) filter, whose response function is shown in Fig. 2. The central frequency correspond to a period of 45 days, with half amplitude at periods of 30 days and 70 days. We have also tested the Lanczos filter (Duchan 1979), and the results are not sensitive. For the master MJO index, we use a western Pacific (0N155E) time series of CMAP precipitation filtered in time as above, but also in space, retaining wavenumbers 0-6. Experiments with more complex space-time filtering (to isolate eastward-propagating components more specifically) suggest that our main findings with respect to vertical structure are robust.

The MJO structure is constructed differently for the COARE and long-term data sets. For the long term data, composite structure is developed by linear regression with respect to the CMAP MJO index. Regressions have been done for all seasons of the year, as well as for individual seasons (December-February, March-May, June-August, and September-November). The confidence level of linear correlation is estimated following Oort and Yienger (1996). In the TOGA COARE data, there are two MJO events (Fig. 3, Chen et al. 1996). We use filtered data on the December 1992 event, a strong MJO event with its amplitude at the TOGA COARE IFA larger than two standard deviation of the 24 year data (Fig. 1a). It moved eastward with a phase speed of 5 m/s, which is similar to the phase speed of the 24 year composite (Fig. 1b). The maximum of the 30-70 day bandpass filtered precipitation anomaly at the TOGA COARE location occurs on December 21, 1992.

4. Heating profiles and stratiform precipitation at the time of maximum precipitation

4.1 Observed heating profile

The vertical heating profiles at the time of maximum precipitation during the MJO life cycle, normalized by surface precipitation, are shown in Fig. 4 for TOGA COARE IFA, OSA and the composites for the winter season (December-February) using 24 years (1979-2002) of chi-corrected heating data. The two TOGA COARE profiles look quite similar with each another, suggesting that the profile is robust with respect to different array size, and different detailed methods for calculating the sounding array budgets. The two profiles are very top-heavy, i.e., with strong heating in the upper troposphere and weak heating in the lower troposphere. The composite MJO profile for the winter season using chi-corrected heating data are similar to the TOGA COARE profiles, except for being a little less top-

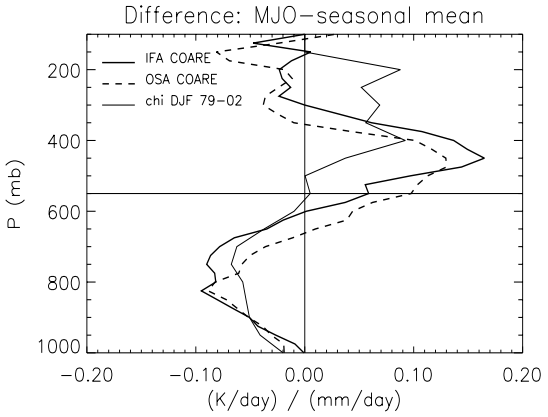

Figure 5: Difference between the MJO anomalous heating profile at the time of maximum precipitation and the seasonal mean profile for TOGA COARE IFA (thick solid line), TOGA COARE OSA (thick dashed line), and DJF composite of 24 years (1979-2002) chi-corrected heating data at 0N155E (thin solid line).

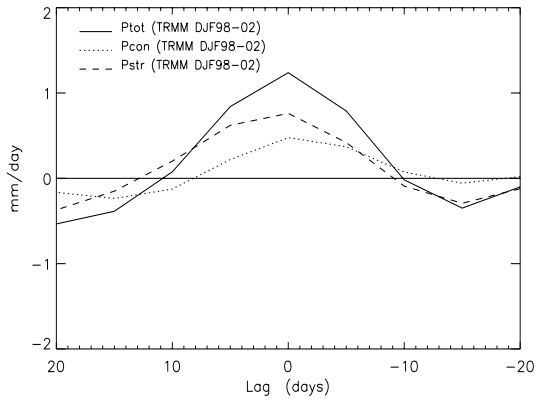

Figure 6: The precipitation anomaly during the DJF MJO composite life cycle for 5 years (1998-2002) of TRMM PR data at 0N155E. The thick solid line is the total precipitation. The thin solid line is the convective precipitation. The thin dashed line is the stratiform precipitation.

heavy, suggesting that the TOGA COARE profiles are statistically representative. For the 4-month period of TOGA COARE, the mean chi-corrected heating profile is almost the same as the rawinsonde-derived profiles (not shown; see Sardeshmuch et al. 1999), suggesting that the modest chi-COARE differences seen here reflect temporal variability, not necessarily error in the chi-corrected heating product. Composites MJO heating profiles for other seasons indicate that the shape of the heating profile has little seasonal variation (not shown).

The difference between the MJO anomaly profile at the time of maximum precipitation and the seasonal mean profile is illustrated in Fig. 5 for both TOGA COARE and chi-corrected heating data. In TOGA COARE, the MJO anomaly profiles are significantly more top-heavy than the seasonal mean profiles, i.e., with stronger heating in the upper troposphere and weaker heating in the lower troposphere. This is also the case for the chi-corrected heating data except with the upper troposphere heating differences located at a higher altitude. The difference profiles are similar to the stratiform heating profiles (Houze 1982, 1989, Johnson 1984), suggesting that the MJO may be associated with larger fraction of stratiform precipitation than the seasonal mean value. To pursue this suggestion, the next section examines the contribution of stratiform precipitation using spaceborne radar data.

4.2 Contribution of stratiform precipitation to the heating profile

Figure 6 shows the precipitation anomaly during the composite MJO life cycle for 5 years (1998-2002) of TRMM precipitation radar (PR) data at 0N, 155E. The thick solid line is total precipitation, the thin solid line is convective precipitation, and the thin dashed line is stratiform precipitation. At the time of maximum precipitation, the stratiform precipitation contributes about 60% of the anomalous total precipitation. The stratiform precipitation lags the convective precipitation by several days, implying a larger fraction of stratiform precipitation in the later stages (examined further in section 5).

The larger stratiform rain fraction in the MJO wet phase, compared to its climatological mean value, is true across longitude (Fig. 7). In both the western Pacific and the eastern Indian Ocean, the stratiform rain fraction in the MJO is about 0.1 larger than its climatological mean value. This finding is consistent with the observation in Fig. 5 that the differences between MJO anomaly heating profiles and seasonal mean profiles are similar in shape to stratiform heating profiles. It is also consistent with previous findings that the MJO modulates larger mesoscale convective systems more than small systems (e.g. Mapes and Houze 1993, Chen et al. 1996), in light of the fact that larger systems have a greater stratiform rain fraction (e.g. Nesbitt et al. 2000). Interestingly, the east-west gradient in stratiform rain fraction across the Pacific (c.f. Schumacher and Houze 2003) is seen in both the MJO anomaly and mean curves in Fig. 7.

For a more quantitative consistency check between the stratiform-rain and heating-profile ob-

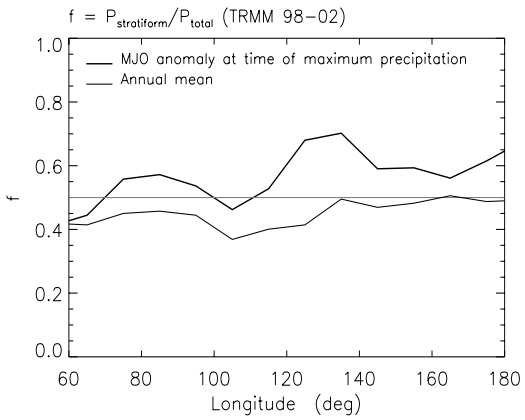

Figure 7: Stratiform rain fraction at the time of maximum precipitation in the composite MJO life cycle (thick line) and the annual mean (thin line) for TRMM PR data along the equator (5N-5S).

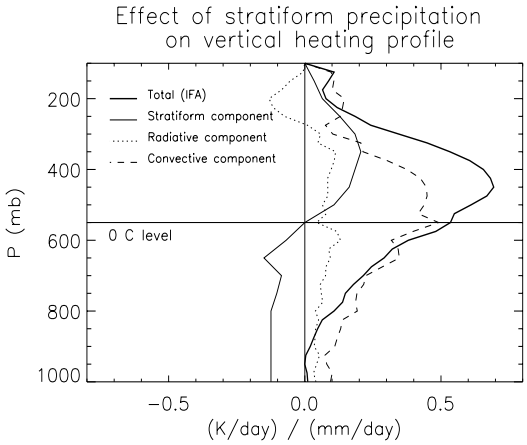

Figure 8: Partition of the observed IFA MJO anomalous heating profile (thick solid line) into three components: the stratiform component (thin solid line), the radiative component (thin dotted line), and the convective component (thin dashed line).

servations, we can formally partition the observed TOGA COARE IFA heating profile into three components: stratiform, radiative and convective, following the method of Johnson (1984):

$$\hat{Q}_1 \approx f\hat{Q}_{1m} + (1-f)\hat{Q}_{1c} + (Q_R/P_0) \qquad (1)$$

where Q_{1m} is the heating in the stratiform precipitation region, Q_{1c} the heating in the convective precipitation region, Q_R the radiative heating, P_0 the area-averaged precipitation rate, and f the stratiform rain fraction. The caret refers to values of Q_1 normalized by surface precipitation rate. Previous observations show good agreement in rainrate-normalized stratiform heating profiles, but diverse results in convective heating profiles (see comparisons by Houze 1989 and Tao et al. 2001). For this reason, Q_{1c} instead of Q_{1m} is derived as a residual.

For the partition, the normalized stratiform heating profile Q_{1m} is taken from Houze (1982), while the intraseasonal Q_R wet-phase anomaly is obtained from the hourly IFA radiative heating profiles calculated by Qian and Cess (2003). The stratiform rain fraction is taken to be 0.6 from Fig. 6. This partition exercise is imperfect, since the stratiform heating profile in Houze (1982) represents the mature phase of strong mesoscale anvils, while the stratiform precipitation reported by TRMM PR includes developing, mature, and decaying phases of mesoscale anvils, as well as the stratiform precipitation not associated with mesoscale convective systems. Nevertheless, the results are adequate for qualitative use.

The partition result is shown in Fig. 8. The convective heating peaks in the middle troposphere near the 0^oC level and only slightly contributes to the top-heaviness of the total profile. The radiative heating is characterized by cloud-top cooling above 250 mb and cloud-base warming below 250 mb, and slightly decreases the top-heaviness of the total profile. The stratiform heating, however, significantly increases the top-heaviness of the total profile. Its upper troposphere heating enhances the convective heating by more than 50%, while its lower troposphere cooling cancels more than 50% of the convective heating. Theoretically, the convective heating can be further divided into two components: net condensation and eddy flux convergence. Considering only the convective heating but not the stratiform heating, Cho and Pendlebury (1997) argued that the only process that might produce a heating maximum in the upper troposphere is the eddy flux convergence, because the net condensation generally has a maximum in the lower troposphere. Fig. 8 shows that the stratiform heating is another major contributor to the upper troposphere heating maximum, and it is more efficient in increasing the top-heaviness because it simultaneously cools the lower troposphere.

5. Vertical phase tilt of heating anomaly

This section extends results from the heating profile at the time of maximum precipitation to the variations of heating profile during the whole MJO life cycle. Figure 9a shows the vertical structure of Q_1 anomaly in TOGA COARE IFA for the December 1992 MJO event, versus time lag (with respect to the time of maximum precipitation, with the axis reversed so that the local time evolution at one longitude visually resembles a spatial cross-section through the eastward-moving MJO (Fig. 3,

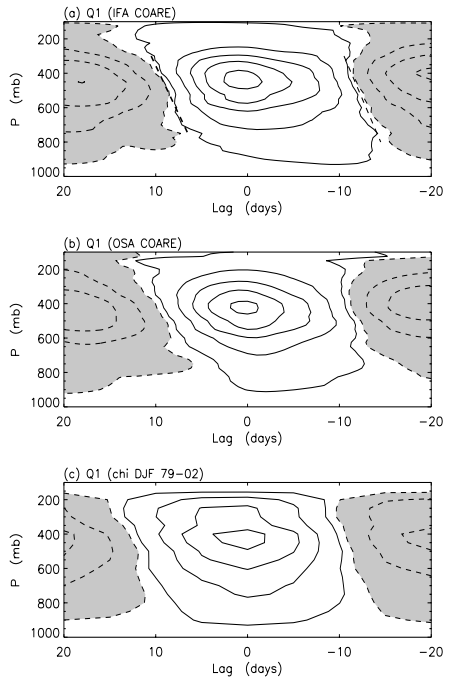

Figure 9: The vertical structure of the diabatic heating anomaly in the MJO for (a) TOGA COARE IFA. (b) TOGA COARE OSA. (c) DJF composite of 24 years (1979-2002) of chi-corrected heating data at 0N155E, normalized by column-integrated heating at the time of maximum precipitation. Unit is (K/day)/(mm/day). Time lag is with respect to the time of maximum precipitation. First contour is 0.03, and contour interval is 0.15. Negative contours are shaded. In (c) only anomaly with linear correlation above 95% confidence level is plotted. In (a) the vertical phase tilts at the leading and trailing edges are highlighted with thick dashed lines.

Fig. 1b).

A subtle but distinct tilt of the heating contours in this time-height section is evident, as highlighted by the thick dashed lines in Fig. 9a at the leading and trailing edges of the positive anomaly. Anomalous heating develops first in the lower troposphere near day -15 and then shifts upward as it intensifies. The maximum heating is below 800 mb before day -10, shifts upward to 450 mb at day 0, and shifts further upward to above 400 mb after day +5. Heating for the TOGA COARE OSA (Fig. 9b), shows similar vertical structure as the IFA, indicating that the vertical heating structure is robust with respect to the different array sizes and calculation methods. These COARE results appear to be statistically representative, as the long-term composite (Fig. 9c) exhibits similar tilt. Composites for other seasons have similar vertical structure as this DJF composite (not shown). To the extent that the MJO propagates past the reference longitude (155E) with nearly fixed structure, these tilted time-height contours correspond to a westward spatial phase tilt of heating with height, as has been found in simulated intraseasonal oscillations in GCMs (Lau et al. 1988, Wang and Schlesinger 1999).

This observed rising of the heating profile with time can be attributed, based on Eq. 1, to one or more of the following three factors: (1) variation of the convective heating $\hat{Q}_{1c}$ profile (i.e. shallower convective heating in the earlier stage and deeper convective heating in later stage); (2) variation of the stratiform heating fraction f (i.e. more stratiform heating in later stage); and (3) variation of the radiative heating Q_R profile. These factors can be separated by the same partitioning exercise used in section 4.2, extended to all the anomalous heating profiles during the MJO life cycle. Assembling the data for this decomposition is a bit tricky, since radiative heating data are only available for COARE while stratiform rain fraction f is only available from TRMM data unavailable during COARE. Here, the variation of stratiform rain is taken from Fig. 6. Radiative heating comes from the computations of Qian and Cess (2003), and convective heating is derived as a residual.

The partitioned heating results are shown in Fig. 10 as a function of lag and height. The derived convective heating (Fig. 10c) has little tilt at the trailing edge of the MJO (positive lags) in the middle and lower troposphere, as highlighted by the thick dashed line. Instead, the tilt of the contours of total heating near day +10 in Fig. 9a is largely due to the extra stratiform heating/cooling couplet at positive lag (Fig. 10b), plus tilted radiative heating (Fig. 10a). This tilted radiative heating is associated with stratiform anvil clouds, including clouds extending well beyond areas of stratiform precipitation. On the other hand, much of the tilt seen in the total heating contours at the MJO's leading edge (lags -15 to -10 days) is exhibited by the convective heating (the thick dashed line at the leading edge is exactly the same as that in Fig. 9a).

The large-scale causes for enhanced stratiform precipitation lagging behind maximum precipitation appear to include wind shear and middle- to upper-troposphere relative humidity. Increasing stratiform rain fraction with vertical wind shear in mesoscale convective systems (MCSs) has been found in both observational studies (Saxen and Rutledge 2000) and numerical modeling studies (Shie et al. 2003). This relationship also holds at the MJO time scale in these COARE and long-term data, as shown in Fig. 11. Both low-level (1000-850mb) shear and deep

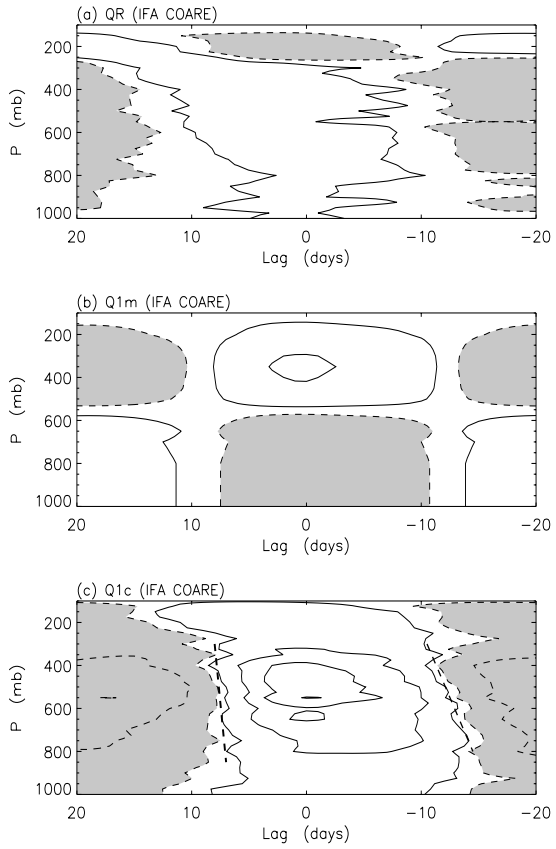

Figure 10: As in Fig. 9 except for TOGA COARE IFA (a) Q_R anomaly, (b) Q_{1m} anomaly, and (c) Q_{1c} anomaly. Contours are the same as in Fig. 9. In (c) the vertical phase tilts at the leading edge and trailing edge are highlighted with thick dashed lines, with the one at the leading edge same as that in Fig. 9a.

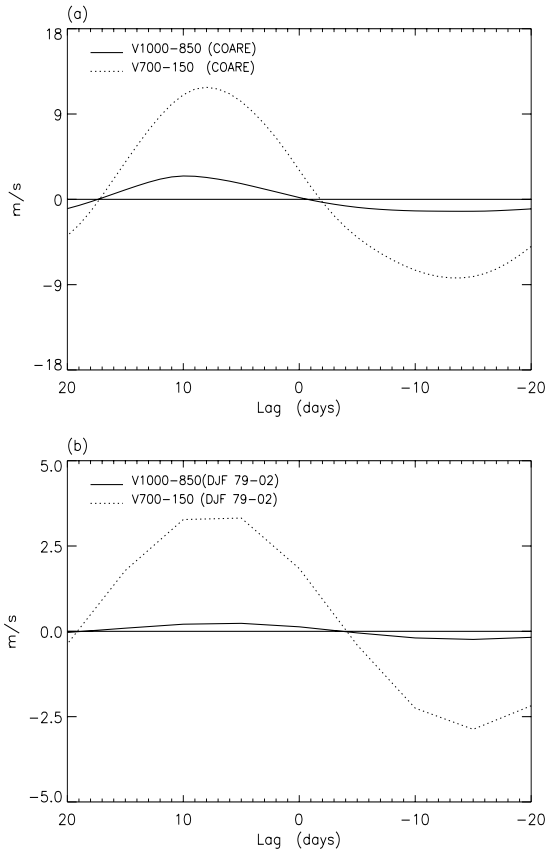

Figure 11: As in Fig. 6 except for vertical wind shear anomaly for (a) TOGA COARE IFA, and (b) DJF composite of 24 years (1979-2002) of NCEP reanalysis data at 0N155E. The solid line is 1000-850 mb wind shear and the dotted line is 700-150 mb wind shear.

(700-150mb) shear lag precipitation by about 5-10 days. In addition to this shear effect, middle- to upper-tropospheric relative humidity may be important. Positive correlations between stratiform rain fraction and humidity in MCSs have been observed by Halverson et al. (1999). A cleaner delineation of cause and effect is found in the cloud modeling work of Tao et al. (1993), who found increases in area coverage and earlier formation of stratiform rain with more humid initial conditions. Similar lags of both stratiform fraction and humidity are seen in these intraseasonal composites (Fig. 12): humidity in the 600-200 hPa layer lags precipitation by 2-5 days in rawinsonde data from both the COARE filtered event data (panel a) and a five year set (1998-2002) of sounding data at the ARM Manus site (2S147E, panel b).

In summary, a distinct tilt is observed in time-height sections of the total heating field at 155E. The data, while noisy, suggest that this tilt may have different causes at the leading and trailing edges of the COARE MJO event: At the leading edge, convective heating deepens with time, while at the trailing edge, the tilt is more a result of increased latent and radiative heating effects in stratiform anvils. These anvils lag the maximum precipitation by a few days, in step with the lags of wind shear and middle-upper troposphere humidity.

6. Comparison to model heating profiles

Global models tend to simulate the MJO poorly. Theoretical studies within the wave-heating feedback framework suggest that the profile of heating is important to the strength and propagation of disturbances, as reviewed more fully in the discussion below. These prior findings motivated the observational study of MJO heating profiles reported here.

A first step toward improving models with observations is to compare of these observed heating profile against model heating profiles, preferably from

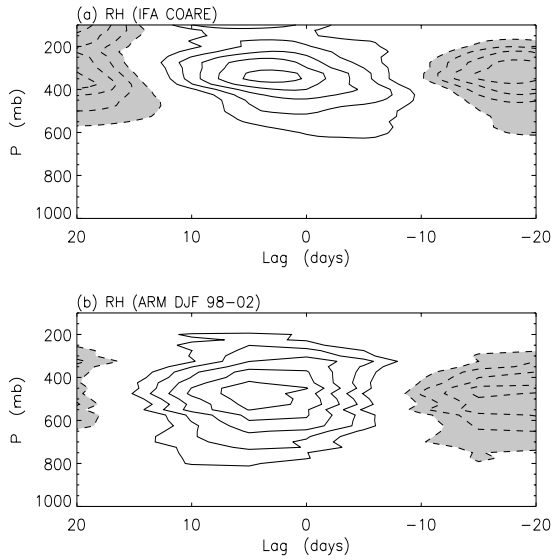

Figure 12: As in Fig. 9 except for RH anomaly for (a) TOGA COARE IFA, and (b) DJF composite of 5 years (1998-2002) of sounding data at ARM Manus site.

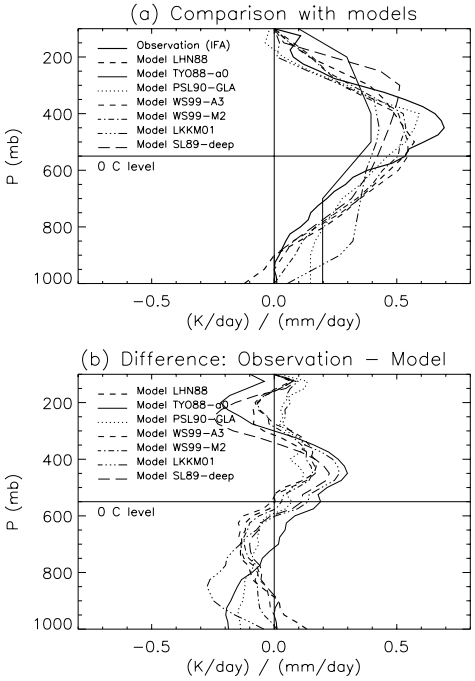

Figure 13: (a) Comparison of the observed heating profile with the model heating profiles. The thick solid line is the observed heating profile. All other lines are the model heating profiles. The models include the GFDL GCM used in Lau et al. 1988 (thick dashed line), the MRI GCM used in Tokioka et al. (1988)'s $\alpha = 0$ experiment (thin solid line), the GLA GCM used in Park et al. 1990 (thin dotted line), the University of Illinois GCM used in Wang and Schlesinger (1999)'s A3 experiment (thin dashed line) and M2 experiment (thin dot-dashed line), the Seoul National University GCM used in Lee et al. 2001 (thin dot-dot-dashed line), and the theoretical model of Sui and Lau (1989)'s deep convection case (thin long-dashed line). (b) The difference between the observed heating profile and the model heating profiles.

multiple models. Obtaining and analyzing model data on all necessary variables with the necessary vertical and time resolution is well beyond the scope of this study. As a smaller step, we surveyed the published literature for all available plots of heating profiles in simulated large-scale equatorial eastward-propagating disturbances. The models include a GFDL GCM (Lau et al. 1988), a Japanese Meteorological Research Institute (MRI) GCM (Tokioka et al. 1988), three GCMs (Goddard Laboratory of Atmospheric Sciences, University of California at Los Angeles, Goddard Laboratory for Atmospheres) compared by Park et al. (1990), the University of Illinois GCM (Wang and Schlesinger 1999), the Seoul National University GCM (Lee et al. 2001), and one idealized model (Sui and Lau 1989). For two papers which show several profiles associated with different GCMs or different experiments with the same GCM (Tokioka et al. 1988, Park et al. 1990), we selected only the most top-heavy profile.

Heating profiles from these seven model studies are displayed in Fig. 13a, along with the observed MJO profile from the COARE IFA data. The mathematical maxima of the model heating profiles vary considerably, as do other, possibly more relevant aspects of profile shape. However, a systematic error is evident: All the model MJO heating profiles are generally middle-heavy, with insufficient heating in the upper troposphere around 450 mb, and excessive heating in the lower troposphere below 600 mb, as highlighted in the difference plot of panel b. In this respect, the differences are similar in shape to the stratiform heating profile (thin solid line in Fig. 8), suggesting that the models systematically lack an intraseasonally-varying stratiform-like heating process.

A model-observation comparison of stratiform rain fraction is not straightforward, or even well-defined. Stratiform precipitation has widely varying definitions even in high-resolution observations and cloud-model data (Lang et al. 2003). It is not clear that any separation of GCM rainfall into "convective" versus "stratiform" parts would correspond meaningfully to any one of the observational separation techniques. In short, we can only say that the models systematically lack a *functional equivalent* of stratiform precipitation.

7. Summary and discussion

This study has examined the top-heaviness of anomalous heating profiles in the MJO, and the related question of stratiform precipitation. Intraseasonal heating profiles simulated by models were compared to the observed. The main findings are:

1. The anomalous vertical heating profile at the time of maximum precipitation is very top-heavy, more so than the climatological mean profile. TRMM data show that anomalous stratiform precipitation contributes about 60% to the intraseasonal precipitation anomaly, more than the climatological fraction of stratiform precipitation. These observations are consistent, in that stratiform precipitation is characterized by heating in the upper troposphere and cooling in the lower troposphere.

2. During the passage of the MJO at 155E, anomalous heating has a phase tilt; that is, the heating maximum rises with time in the heating profile. At the trailing edge of the rainy phase, this tilt is made up largely by latent and radiative heating in stratiform anvils. Heating by these stratiform anvils lags the total precipitation by a few days, associated with the similar lags of vertical wind shear and middle-upper troposphere relative humidity.

3. The anomalous vertical heating profiles in 7 model intraseasonal oscillations differ from observations, in the sense of being middle-heavy rather than top-heavy. Models systematically lack (or underrepresent) some functional equivalent of the observed strong modulation of stratiform precipitation by the MJO.

Is this systematic heating-profile error in models related to their poor simulations of the MJO? We will not presume to offer a simple or definitive answer, but theoretical studies offer some guidance for discussion. As mentioned in the introduction, such studies typically assume a wave-heating feedback framework. The heating in wave-heating feedback theories may be divided into five components, namely the latent heatings associated with free troposphere moisture convergence; boundary layer moisture convergence; surface heat flux (latent plus sensible); and local moisture storage, as well as radiative heating. These five components have been emphasized in different types of theories, including the wave-CISK (Convective Instability of the Second Kind) mechanism (e.g. Hayashi 1970, Lindzen 1974, Lau and Peng 1987, Zhang and Geller 1994), the frictional wave-CISK mechanism (e.g. Hayashi 1971, Wang and Rui 1990b, Salby et al. 1994), the WISHE (Wave Induced Surface Heat Exchange) mechanism (e.g. Emanuel 1987, Neelin et al. 1987), the charge-discharge mechanism (e.g. Blade and Hartmann 1993, Wang and Schlesinger 1999), and the cloud-radiation interaction mechanism (Hu and Randall 1994, Raymond 2001, Lee et al. 2001), respectively.

The role of the vertical heating profile in setting the strength and phase speed of intraseasonal oscillations has been studied in several works. In some theories, such as wave-CISK, the heating profile is specified outright, allowing direct study of the influence of profile shape (Yamasaki 1968a, 1968b, 1969, Lau and Peng 1987, Takahashi 1987, Lau et al. 1988, Chang and Lim 1988, Tokioka et al. 1988, Sui and Lau 1989, Cho and Pendlebury 1997). Two distinct issues accessible to such a treatment are the instability properties (or growth rate) of oscillations, and their phase speeds.

On the question of instability, Cho and Pendlebury (1997) found that instability requires a sufficient amplitude of a full-wave Fourier component to the heating profile - essentially, the 'stratiform' heating profile discussed in this paper. A 'stratiform instability' mechanism is also active in the model of Mapes (2000). Yamasaki (1968a, 1968b, 1969) found in numerical modeling studies that some tropical systems are unstable only if the cumulus heating profile has a maximum in the upper troposphere. On the basis of these results, a systematic lack of stratiform-like heating in models could be hypothesized to contribute to too-weak intraseasonal variability.

On the question of phase speed, results are available from several wave-CISK studies using linearized heating (Takahashi 1987, Lau et al. 1988) or conditional ("positive only") heating (Lau and Peng 1987, Sui and Lau 1989). In all cases, phase speed is found to increase with increases in the altitude of the maximum heating rate. A consistent result from a full GCM study is that of Tokioka et al. (1988), who introduced a critical (minimum) entrainment rate to the Arakawa-Schubert convection scheme. As this critical parameter was increased, both the altitude of the maximum heating and the phase speed of simulated intraseasonal oscillations decreased. Another GCM result in the same sense is Park et al. (1990)'s comparison of simulated intraseasonal oscillations in three different GCMs.

By these results, the too-fast propagation of intraseasonal oscillation in models would not seem to be attributable to their systematic heating-profile bias, since the effect appears to be of the wrong sign. However, it is not clear that the theoretical results are as consistent as they appear, since the altitude of peak heating isn't necessarily the salient feature of heating profiles. From the perspective of adiabatic Kelvin wave dynamics, a heating profile should be characterized by what vertical modes it

excites. Waves of short vertical wavelength, which propagate slowly, are excited by heating that is either top-heavy or bottom-heavy. If such waves play a role in the slow phase speed of the MJO, a simple peak-altitude characterization of heating may be misleading. Moreover, the large-scale circulation ('wave') structure of the observed MJO resembles a combination of forced-damped Kelvin and Rossby wave responses to equatorial heating (e.g. Kiladis and Weickmann 1992, Hsu 1996), which is similar to the Gill pattern (Gill 1980), not the pure Kelvin wave used in many theoretical models. As shown by Wheeler and Kiladis (1999), the spectral power of the MJO does not lie along a Kelvin wave dispersion curve. Convectively-coupled Kelvin waves exist, distinct from the MJO, and propagate faster (10-15 m/s). Instead of "too-fast" MJOs, perhaps many models have reasonable or even too-slow convectively coupled Kelvin waves, and lack the MJO entirely! To summarize this discussion, there is plenty of suggestive literature but no really satisfying basis to conclude that models' systematic errors in heating profiles and intraseasonal oscillation propagation speed are linked.

The difficulties of attempting to link heating and MJO simulation should not be allowed to distract from the striking consistency found among model heating-profile errors (Fig. 13b). This finding suggests there may be a fundamental problem common to many models, which certainly merits attention. Systematic model errors continue to frustrate MJO research, as it is hard to find a model, much less a suite of models, with variability sufficiently similar to observations to permit comparative studies to lead to incremental improvements. Vertical structure seems to contain important clues to the linkages between large-scale horizontal patterns (like MJO development and propagation) and physical processes, and this observational study provides a baseline.

Acknowledgments. Part of this work was done during the first author's Ph.D study. Helpful discussions with the late Dr. Yoshikazu Hayashi, David Randall, Robert Cess, Sultan Hameed, Marvin Geller, and Yogesh Sud are gratefully acknowledged, along with helpful reviews of the original manuscript by George Kiladis, Robert Houze, Steve Rutledge, Richard Johnson, and two anonymous reviewers. The TOGA COARE IFA sounding array budgets were provided by Paul Ciesielski and Richard Johnson, while radiative heating profile data were generously shared by Taotao Qian and Robert Cess in advance of their publication elsewhere. This work was supported by National Science Foundation grants ATM-0073206 and ATM-0112715, and by NOAA/OGP and CDC.

REFERENCES

Bergman, J. W., H. H. Hendon, K. M. Weickmann, 2001: Intraseasonal Air-Sea Interactions at the Onset of El Nino. *J. Climate*, **14**, 1702-1719.

Blade, I., and D. L. Hartmann, 1993: Tropical intraseasonal oscillations in a simple nonlinear model. *J. Atmos. Sci.*, **50**, 2922-2939.

Chang, C. P., and H. Lim, 1988: Kelvin wave-CISK: A possible mechanism for the 30-50 day oscillations. *J. Atmos. Sci.*, **45**, 1709-1720.

Chen, S. S., R. A. Houze., and B. E. Mapes, 1996: Multiscale variability of deep convection in relation to large-scale circulation in TOGA COARE. *J. Atmos. Sci.* , **53**, 1380-1409.

Cho, Han-Ru, D. Pendlebury, 1997: Wave CISK of Equatorial Waves and the Vertical Distribution of Cumulus Heating. *J. Atmos. Sci.*, **54**, 2429-2440.

Ciesielski, P. E., R. H. Johnson, and J. Wang, 2002: Impacts of humidity-corrected sonde data on TOGA COARE analyses. *Preprints, 25th Conference on Hurricanes and Tropical Meteorology*, 29 April - 3 May 2002, San Diego, CA.

Duchan, C.E., 1979: Lanczos filtering in one and two dimensions. *J. Appl. Meteor.*, **18**, 1016-1022.

Emanuel, K. A., 1987: An air-sea interaction model of intraseasonal oscillation in the Tropics. *J. Atmos. Sci.*, **44**, 2324-2340.

Frank, W. M., and J. L. McBride, 1989: The vertical distribution of heating in AMEX and GATE cloud clusters. *J. Atmos. Sci.*, **46**, 3464-3478.

Frank, W. M., H. Wang, and J. L. McBride, 1996: Rawinsonde budget analyses during the TOGA COARE IOP. *J. Atmos. Sci.*, **53**, 1761-1780.

Gill, A. E., 1980: Some simple solutions for heat-induced tropical circulation. *Quart. J. Roy. Meteor. Soc.*, **106**, 447-462

Halverson, J. B., B. S. Ferrier, T. M. Rickenbach, J. Simpson, and W.-K. Tao, 1999: An ensemble of convective systems on 11 February 1993 during TOGA COARE: Morphology, rain characteristics, and anvil cloud interactions. *Mon. Wea. Rev.*, **127**, 1208-1228.

Hayashi, Y., and A. Sumi, 1986: The 30-40 day oscillation simulated in an"aqua planet" model. *J. Meteor. Soc. Japan.*, **64**, 451-466.

Hayashi, Y., 1970: A theory of large-scale equatorial waves generated by condensation heat and accelerating the zonal wind. *J. Meteor. Soc. Japan*, **48**, 140-160.

Hayashi, Y., 1971: Large-scale equatorial waves destabilized by convective heating in the presence of surface friction. *J. Meteor. Soc. Japan*, **49**, 458-466.

Hayashi, Y., and D. G. Golder, 1986: Tropical intraseasonal oscillations appearing in a GFDL general circulation model and FGGE data. Part I: Phase propagation.

J. Atmos. Sci., **43**, 3058-3067.

Hayashi, Y., and D. G. Golder, 1988: Tropical intraseasonal oscillations appearing in a GFDL general circulation model and FGGE data. Part II: Structure. *J. Atmos. Sci.*, **45**, 3017-3033.

Hendon, H. H., and B. Liebmann, 1990: A composite study of onset of the Australia monsoon. *J. Atmos. Sci.*, **47**, 2227-2240.

Hendon, H. H., and M. L. Salby, 1994: The life cycle of the Madden-Julian oscillation. *J. Atmos. Sci.*, **51**, 2225-2237.

Higgins, R. Wayne, Kingtse C. Mo, 1997: Persistent North Pacific Circulation Anomalies and the Tropical Intraseasonal Oscillation. *J. Climate*, **10**, 223-244.

Higgins, R. W., J.-K. E. Schemm, W. Shi, A. Leetmaa, 2000: Extreme Precipitation Events in the Western United States Related to Tropical Forcing. *J. Climate*, **13**, 793-820.

Houze, R. A., 1982: Cloud clusters and large-scale vertical motions in the Tropics. *J. Meteor. Soc. Japan*, **60**, 396-410.

Houze, R. A., 1989: Observed structure of mesoscale convective systems and implications for large-scale heating. *Quart. J. Roy. Meteor. Soc.*, **115**, 425-461.

Houze, R. A., 1997: Stratiform precipitation in regions of convection: A meteorological paradox? *Bull. Amer. Meteor. Soc.*, **78**, 2179-2196.

Hsu, H.-H., 1996: Global view of the intraseasonal oscillation during northern winter. *J. Climate*, **9**, 2386-2406.

Hu, Q., and D. A. Randall, 1994: Low-frequency oscillations in radiative-convective systems. *J. Atmos. Sci.*, **51**, 1089-1099.

Johnson, R. H., 1984: Partitioning tropical heat and moisture budgets into cumulus and meso-scale components: Implication for cumulus parameterization. *Mon. Wea. Rev.*, **112**, 1590-1601.

Kessler, W. S., and M. J. McPhaden, and K. M. Weickmann, 1995: Forcing of intraseasonal Kelvin waves in the equatorial Pacific. *J. Geophys. Res.*, **100**, 10613-10631.

Kiladis, G. N., and K. M. Weickmann, 1992: Circulation anomalies associated with tropical convection during northern winter. *Mon. Wea. Rev.*, **120**, 1900-1923.

Knutson, T. R., and K. M. Weickmann, 1987: 30-60 day atmospheric oscillations: Composite life cycles of convection and circulation anomalies. *Mon. Wea. Rev.*, **115**, 1407-1436.

Krishnamurti, T.-N., P. K. Jayakumar, J. Sheng, N. Surgi, and A. Kuma, 1985: Divergent circulations on the 30 to 50 day timescale. *J. Atmos. Sci.*, **42**, 364-375.

Kummerow, C., J. Simpson, O. Thiele, W. Barnes, A. T. C. Chang, E. Stocker, R. F. Adler, A. Hou, R. Kakar, F. Wentz, P. Ashcroft, T. Kozu, Y. Hong, K. Okamoto, T. Iguchi, H. Kuroiwa, E. Im, Z. Haddad, G. Huffman, B. Ferrier, W. S. Olson, E. Zipser, E. A. Smith, T. T. Wilheit, G. North, T. Krishnamurti, K. Nakamura, 2000: The Status of the Tropical Rainfall Measuring Mission (TRMM) after Two Years in Orbit. *J. of Appl. Meteor.*, **39**, 1965-1982.

Lang, S., W.-K. Tao, J. Simpson, and B. Ferrier, 2003: Modeling of convective-stratiform precipitation processes: sensitivity to partitioning methods. *J. Appl. Meteor.*, **42**, 505-527.

Lau, K. M., and P. H. Chan, 1985: Aspects of the 40-50-day oscillation during the northern winter as inferred from outgoing longwave radiation. *Mon. Wea. Rev.*, **113**, 1889-1909.

Lau, K. M., and L. Peng, 1987: Origin of low-frequency (intraseasonal) oscillations in the tropical atmosphere. *J. Atmos. Sci.*, **44**, 950-972.

Lau, K.-M., and T. J. Phillips, 1986: Coherent fluctuations of extratropical geopotential height and tropical convection in intraseasonal timescales. *J. Atmos. Sci.*, **43**, 1164-1181.

Lau, N. C., I. M. Held, and J. D. Neelin, 1988: The Madden-Julian oscillations in an idealized general circulation model. *J. Atmos. Sci.*, **45**, 3810-3831.

Lee, M.-I., I.-S. Kang, J.-K. Kim, and B.E. Mapes, 2001: Influence of cloud-radiation interaction on simulating tropical intraseasonal oscillation with an atmospheric general circulation model , *J. Geophys. Res.*, **106**, 14219-14233.

Liebmann, B., H. H. Hendon, and J. D. Glick, 1994: The relationship between tropical cyclones of the western Pacific and Indian Oceans and the Madden-Julian oscillation. *J. Meteor. Soc. Japan*, **72**, 401-411.

Lin, X., and R. H. Johnson, 1996: Heating, moistening, and rain over the western Pacific warm pool during TOGA COARE. *J. Atmos. Sci.*, **53**, 3367-3383.

Lindzen, R. E., 1974: Wave-CISK in the tropics. *J. Atmos. Sci.*, **31**, 156-179.

Madden, R. A., and P. R. Julian, 1971: Detection of a 40-50 day oscillation in the zonal wind in the tropical Pacific. *J. Atmos. Sci.*, **28**, 702-708.

Madden, R. A., and P. R. Julian, 1972: Description of global-scale circulation cells in the tropics with a 40-50 day period. *J. Atmos. Sci.*, **29**, 1109-1123.

Madden, R. A., and P. R. Julian, 1994: Observations of the 40-50-day tropical oscillation-A review. *Mon. Wea. Rev.*, *122*, 814-837.

Mapes, B. E., 2000: Convective inhibition, subgrid-scale triggering energy, and stratiform instability in a toy tropical wave model. *J. Atmos. Sci.*, **57**, 1515-1535.

Mapes, B. E., and R. A. Houze, 1993: Cloud clusters and superclusters over the oceanic warm pool. *Mon. Wea. Rev.*, **121**, 1398-1415.

Mapes, B. E., and R. A. Houze, 1995: Diabatic divergence profiles in western Pacific mesoscale convective systems. *J. Atmos. Sci.*, **52**, 1807-1828.

McAnelly, R. L., and W. R. Cotton, 1989: The precipitation lifecycle of mesoscale convective complexes over the central United States. *Mon. Wea. Rev.*, **117**, 784-808.

Murakami, M., 1979: Large-scale aspects of deep convective activity over the GATE area. *Mon. Wea. Rev.*, **107**, 994-1013.

Murakami, T., and T. Nakazawa, 1985: Tropical 45 day oscillation during the 1979 Northern Hemisphere summer. *J. Atmos. Sci.*, **42**, 1107-1122.

Nakazawa, T., 1986: Intraseasonal variations in the OLR in the Tropics during the FGGE year. *J. Meteor. Soc. Japan*, **64**, 17-34.

Neelin, J. D., I. M. Held, and K. H. Cook, 1987: Evaporation-wind feedback and low-frequency variability in the tropical atmosphere. *J. Atmos. Sci.*, **44**, 2341-2348.

Nesbitt, S. W., Zipser, E. J., Cecil, and D. J. 2000: A Census of Precipitation Features in the Tropics Using TRMM: Radar, Ice Scattering, and Lightning Observations. *J. Climate*, **13**, 4087-4106.

Oort, A. H., and J. J. Yienger, 1996: Observed long-term variability in the Hadley circulation and its connection to ENSO. *J. Climate*, **9**, 2751-2767.

Park, C. K., D. M. Straus, and K.-M. Lau, 1990: An evaluation of the structure of tropical intraseasonal oscillations in three general circulation models. *J. Meteor. Soc. Japan*, **68**, 403-417.

Qian, T., and R. D. Cess, 2003: Cloud vertical structure and radiative heating profiles during TOGA COARE. manuscript in preparation.

Raymond, D. J., 2001: A New Model of the Madden-Julian Oscillation. *J. Atmos. Sci.*, **58**, 2807-2819.

Rui, H., and B. Wang, 1990: Development characteristic and dynamic structure of tropical intraseasonal convection anomalies. *J. Atmos. Sci.*, **47**, 357-379.

Salby, M. L., and H. H. Hendon, 1994: Intraseasonal behavior of clouds, temperature, and motion in the Tropics. *J. Atmos. Sci.*, **51**, 2207-2224.

Salby, M. L., R. B. Garcia, and H. H. Hendon, 1994: Planetary-scale circulations in the presence of climatological and wave-induced heating. *J. Atmos. Sci.*, **51**, 2344-2367.

Sardeshmukh, P. D., 1993: The baroclinic problem and its application to the diagnosis of atmospheric heating rates. *J. Atmos. Sci.*, **50**, 1099-1112.

Sardeshmukh, P. D., M. Newman, and C. R. Winkler, 1999: Dynamically consistent estimates of diabatic heating. *Proceedings, 24th Climate Diagnostics and Prediction Workshop*, Tucson, AZ, 172-175. Also available at http://www.cdc.noaa.gov/map/chi/discussion.html

Saxen, T. R., and S. A. Rutledge, 2000: Surface Rainfall-Cold Cloud Fractional Coverage Relationship in TOGA COARE: A Function of Vertical Wind Shear. *Mon. Wea. Rev.*, **128**, 407-415.

Schumacher, Courtney, Houze, Robert A. 2003: Stratiform Rain in the Tropics as Seen by the TRMM Precipitation Radar. *J. Climate*, **16**, 1739-1756.

Shie, C.-L., W.-K. Tao, J. Simpson, and C.-H. Sui, 2003: Quasi-equilibrium states in the tropics simulated by a cloud-resolving model. Part I: Specific features and budget analysis. *J. Climate*, **16**, 817-833.

Slingo, J. M., and Coauthors, 1996: Intraseasonal oscillations in 15 atmospheric general circulation models: Results from an AMIP diagnostic subproject. *Climate Dyn.*, **12**, 325-357.

Stocker, E., J. Kwiatkowski, O. Kelley, 2001: Gridded Hourly Text Products: A TRMM Data Reduction approach. *Proceedings of IGARSS 2001*, Sydney Australia, 9-13 July 2001.

Sui, C. H., and K.-M. Lau, 1989: Origin of low-frequency (intraseasonal) oscillations in the tropical atmosphere. Part II. Structure and propagation of mobile wave-CISK modes and their modification by lower boundary forcings. *J. Atmos. Sci.*, **46**, 37-56.

Takahashi, M., 1987: A theory of the slow phase speed of the intraseasonal oscillation using wave-CISK. *J. Meteor. Soc. Japan*, **65**, 43-49.

Takayabu, Y .N., T. Iguchi, M. Kachi, A. Shibata, and H. Kanzawa, 1999: Abrupt termination of the 1997-98 El Nino in response to a Madden-Julian oscillation. *Nature*, **402**, 279-282.

Tao, W. K., and J. Simpson, C.-H. Sui, B. Ferrier, S. Lang, J. Scala, M.-D. Chou , and K. Pickering, 1993: Heating, moisture, and water budgets of tropical and midlatitude squall lines: Comparisons and sensitivity to longwave radiation. *J. Atmos. Sci.*, **50**, 673-690.

Tao, W.-K., Lang, S., Olson, W. S., Meneghini, R., Yang, S., Simpson, J., Kummerow, C., Smith, E., Halverson, J. 2001: Retrieved Vertical Profiles of Latent Heat Release Using TRMM Rainfall Products for February 1998. *J. Appl. Meteor.*, **40**, 957-982.

Thompson, R. M., S. W. Payne, E. E. Recker, and R. J. Reed, 1979: Structure and properties of synoptic-scale wave disturbances in the Intertropical Convergence Zone of the eastern Atlantic. *J. Atmos. Sci.*, **36**, 53-72.

Tokioka, T., K. Yamazaki, A. Kitoh, and T. Ose, 1988: The equatorial 30-60-day oscillation and the Arakawa-Schubert penetrative cumulus parameterization. *J. Meteor. Soc. Japan*, **66**, 883-901.

Wang, B., and H. Rui, 1990a: Synoptic climatology of transient tropical intraseasonal convection anomalies. *Meteor. Atmos. Phys.*, **44**, 43-61.

Wang, B., and H. Rui, 1990b: Dynamics of the coupled moist Kelvin-Rossby wave on an equatorial B-plane. *J. Atmos. Sci.*, **47**, 398-413.

Wang, W., and M. E. Schlesinger, 1999: The dependence on convection parameterization of the tropical intraseasonal oscillation simulated by the 11-layer UIUC atmospheric GCM. *J. Climate*, **12**, 1423-1457.

Weickmann, K., 1983: Intraseasonal circulation and outgoing longwave radiation modes during northern winter. *Mon. Wea. Rev.*, **111**, 1838-1858.

Weickmann, K. M., G. R. Lussky, and J. E. Kutzbach, 1985: Intraseasonal (30-60 day) fluctuations of outgoing longwave radiation and 250 mb streamfunction during northern winter. *Mon. Wea. Rev.*, **113**, 941-961.

Wheeler, M., and G. N. Kiladis, 1999: Convectively coupled equatorial waves: Analysis of clouds and temperature in the wavenumber-frequency domain. *J. Atmos. Sci.*, **56**, 374-399.

Winkler, C. R., M. Newman, and P. D. Sardeshmukh, 2001: A linear model of wintertime low-frequency variability. Part I: Formulation and forecast skill. *J. Climate*, **14**, 4474-4494.

Woolnough, S. J., Slingo, J. M., Hoskins, B. J.. 2000: The Relationship between Convection and Sea Surface

Temperature on Intraseasonal Timescales. *J. Climate*, **13**, 2086-2104.

Xie, P., and P. A. Arkin, 1997: Global precipitation: A 17-year monthly analysis based on gauge observations, satellite estimates, and numerical model outputs. *Bull. Amer. Meteor. Soc.*, **78**, 2539-2558.

Yamasaki, M., 1968a: A tropical cyclone model with parameterized partition of released latent heat. *J. Meteor. Soc. Japan*, **46**, 202-214.

Yamasaki, M., 1968b: Detailed analysis of a tropical cyclone simulated with a 13-layer model. *Pap. Meteor. Geophys.*, **19**, 559-585.

Yamasaki, M., 1969: Large-scale disturbances in a conditionally unstable atmosphere in low latitudes. *Pap. Meteor. Geophys.*, **20**, 289-336.

Yanai, M., S. Esbensen, and J.-H. Chu, 1973: Determination of bulk properties of tropical cloud clusters from large-scale heat and moisture budgets. *J. Atmos. Sci.*, **30**, 611-627.

Yanai, M., B. Chen, and W.-W. Tung, 2000: The Madden-Julian oscillation observed during the TOGA COARE IOP: Global view. *J. Atmos. Sci.*, **57**, 2374-2396.

Yasunari, T., 1979: Cloudiness fluctuations associated with the northern hemisphere summer monsoon. *J. Meteor. Soc. Japan*, **57**, 227-242.

Zhang, C., 1996: Atmospheric intraseasonal variability at the surface in the tropical western Pacific Ocean. *J. Atmos. Sci.*, **53**, 739-758.

Zhang, M. H., and M. A. Geller, 1994: Selective excitation of tropical atmospheric waves in wave-CISK: The effect of vertical wind shear. *J. Atmos. Sci.*, **51**, 353-368.

Zhang, M. H., and J. L. Lin, 1997: Constrained variational analysis of sounding data based on column-integrated budgets of mass, heat, moisture, and momentum: Approach and application to ARM measurements. *J. Atmos. Sci.*, **54**, 1503-1524.

Zhang, M. H., and J. L. Lin, 1999: Synthesizing TOGA COARE measurements in the atmosphere, at the surface, and at TOA. *COARE-98. Proc. Conf. on the TOGA Coupled Ocean-Atmosphere Response Experiment (COARE).* Boulder CO, 7-14 July 1998. WMO/TD 940, 309-310.